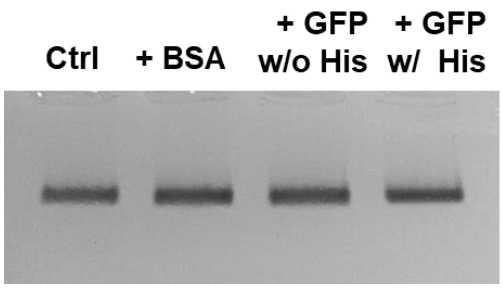

Figure S1. An agarose gel image of 10 nm NTA–AuNP (without Ni charging) binding with various proteins. BSA, 6His-cleaved GFP and 6His-GFP were mixed with 10 nm NTA–AuNP. Ctrl = 10 nm NTA-AuNP.

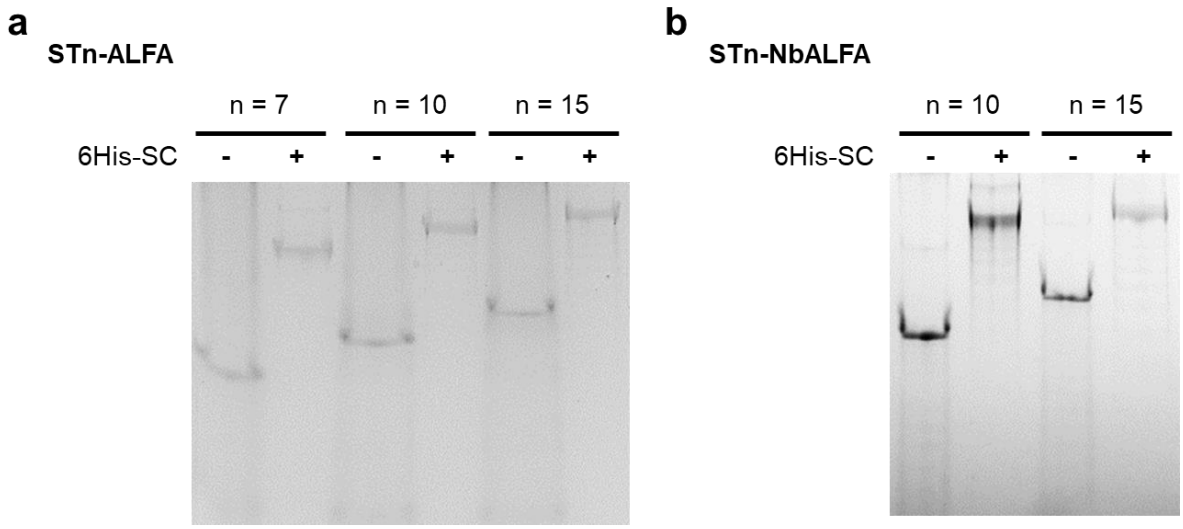

Figure S2. Preparation of 6His-SC-STn chains with various lengths (n) and various (N-or C-terminal) functional proteins. (a) A native gel image of STn-ALFA Tag protein chains (STn with genetically fused ALFA Tag on N-terminal) and their 6His-SC bound forms (6His-SC-STn-ALFA). (b) A native gel image of STn-NbALFA (NbALFA: ALFA-tag binding nanobody) protein chains (STn with genetically fused NbALFA on N-terminal) and their 6His-SC bound forms (6His-SC-STn-ALFA).

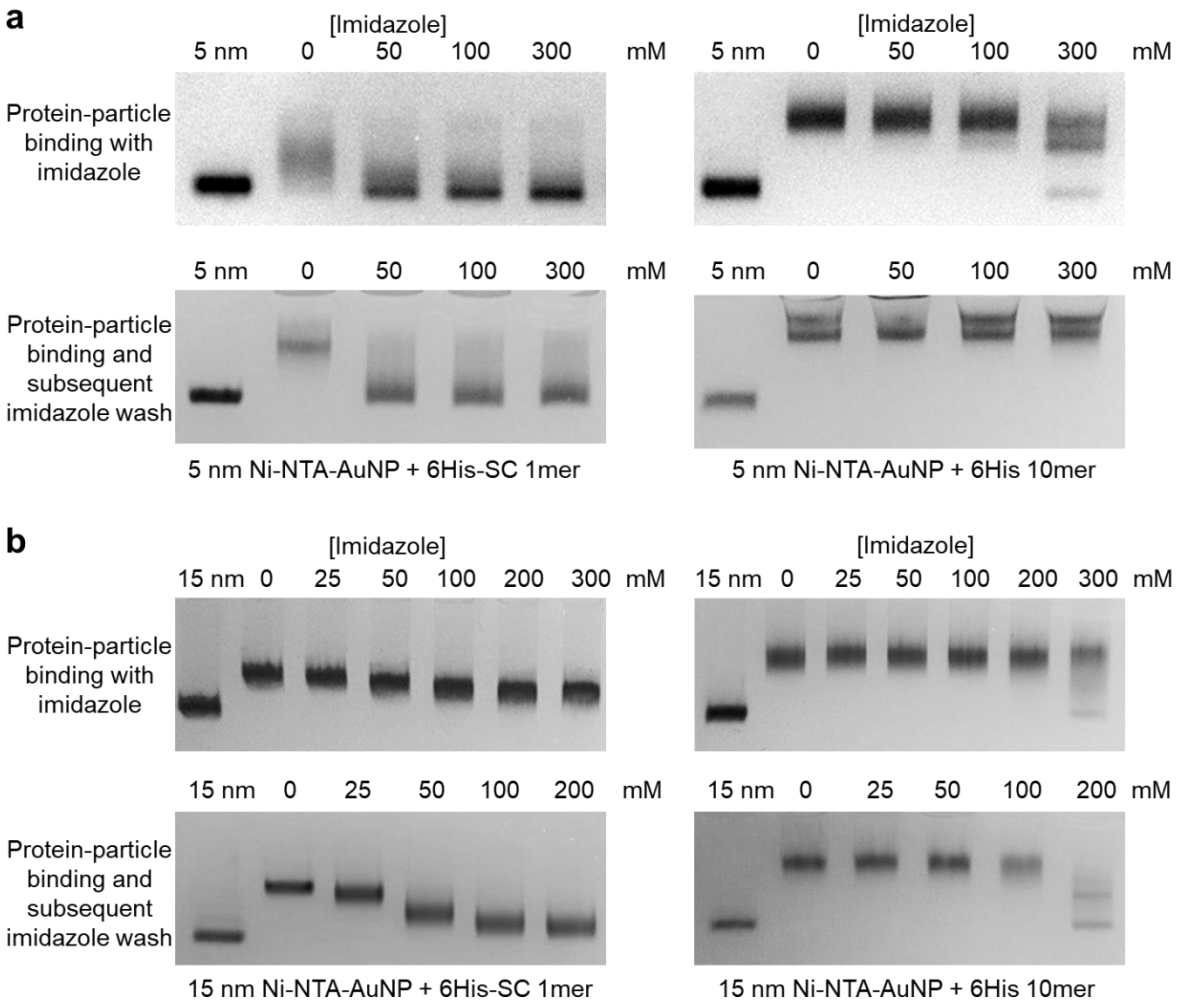

Figure S3. Association and dissociation patterns of 6His monomer and 6His 10mer binding to Ni-NTA-AuNP under different imidazole concentrations. (a) Agarose gel shift analysis of 5 nm Ni-NTA-AuNP binding with 6His-SC monomer (left) or with 6His 10mer (right). Protein-particle binding was conducted with different imidazole concentrations from 0 to 300 mM (top) or without imidazole and subsequently washed with different imidazole concentrations from 0 to 300 mM (bottom). (b) Agarose gel shift analysis of 15 nm Ni-NTA-AuNP binding with 6His-SC monomer (left) or with 6His 10mer (right).

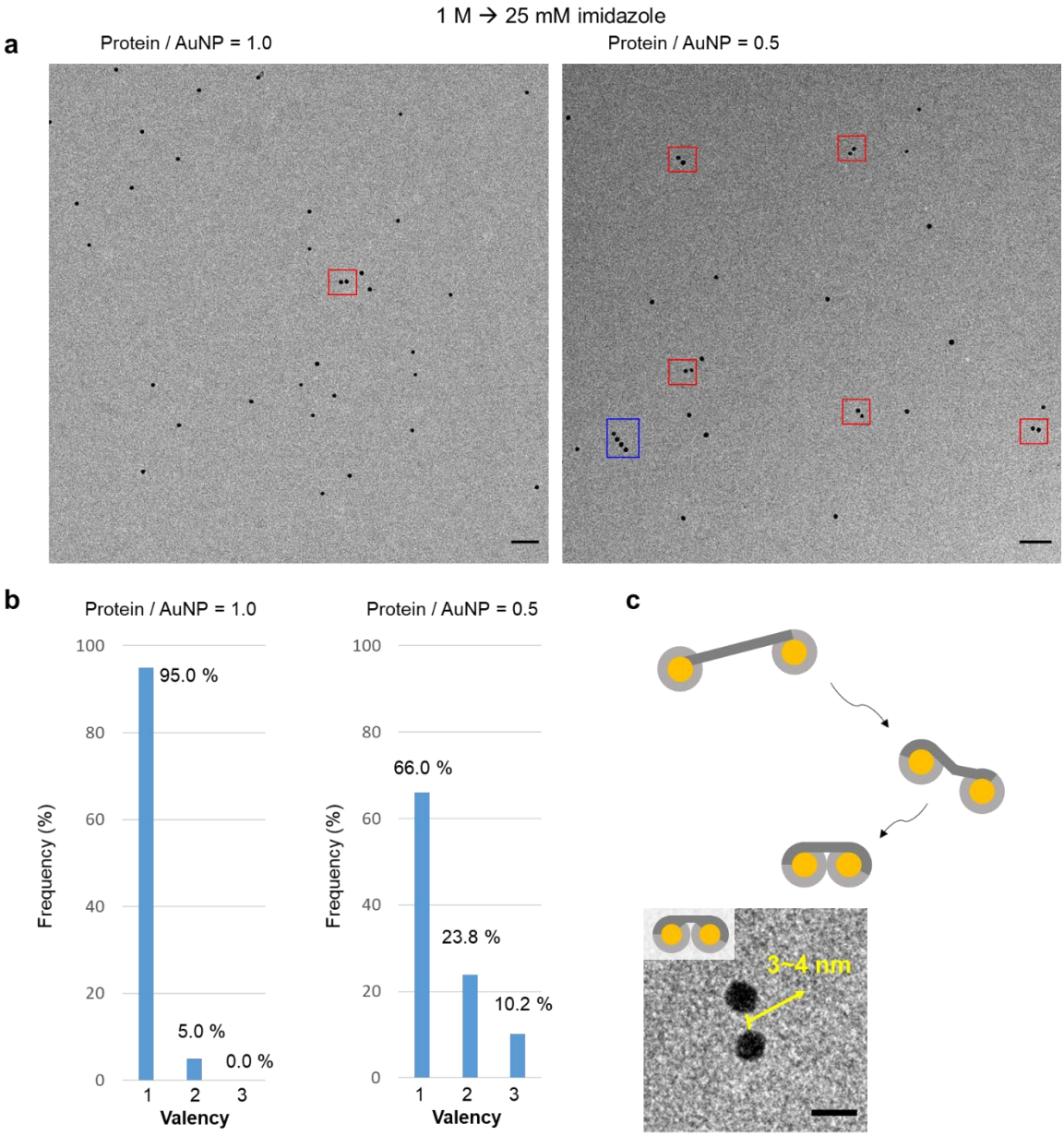

Figure S4. 5 nm Ni-NTA-AuNP bound with 6His-SC-ST15-NbALFA protein under different protein:particle ratios. (a) Wide field TEM images of 5 nm Ni-NTA-AuNP binding to 6His 15mer with slowly decreasing imidazole concentration (from 1 M to 25 mM) at protein:particle ratios 1:1 (left) or at 0.5:1 (right). Dimeric particle assemblies were indicated with red boxes, and higher particle assemblies were indicated with a blue box. Scale bar = 50 nm. (b) Population graphs of protein-bound AuNPs. Protein conjugated particles were classified as monomeric (valency 1), dimeric (valency 2), and trimeric (valency 3) clusters. Over 100 particles in TEM images were examined, and particles that are separated by less than 4 nm were considered as clustered. (c) Schematic illustration and a representative TEM image of dimeric 5 nm Ni-NTA AuNP with conjugated 6His-SC-ST15-NbALFA. AuNP (yellow circle), Ni-NTA coating (light gray), and protein chains (dark gray) are schematically indicated. Scale bar = 10 nm.

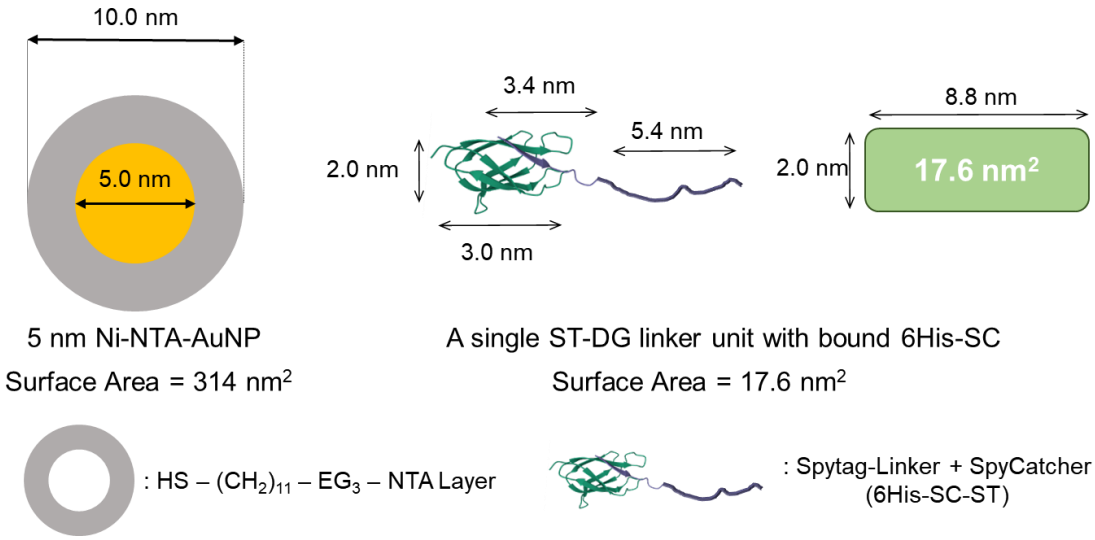

Figure S5. Theoretical sizes of 5 nm Ni-NTA–AuNP and a 6His-SC-ST-linker unit. The diameter of 5 nm Ni-NTA-AuNP is approximated as 10 nm by considering a NTA layer (gray). A SC-ST complex size was estimated based on the crystal structure of the SC-ST complex (PDB: 4MLI), and the length of the 16 residue peptide linker (DGDGDGDGDGLVPRGS) was estimated by assuming that it is fully extended (10 amino acids: ~3.4 nm).

Supplementary Note I: Assuming that there is no overlaps between units, the approximate maximal binding number for the SC unit on 5 nm Ni-NTA-AuNP is calculated as 17.84 (314 nm^2/17.6 nm^2). However, it is also possible that SC-ST complexes occupy more surface space due to repulsion (decrease the maximal binding number), or the 16 residue peptide linker is not fully extended (increase the maximal binding number).

Supplementary Note II: Similarly, surface areas of 10 nm Ni-NTA-AuNP and 15 nm Ni-NTA-AuNP can be calculated as 706.5 nm^2 and 1256 nm^2, respectively.

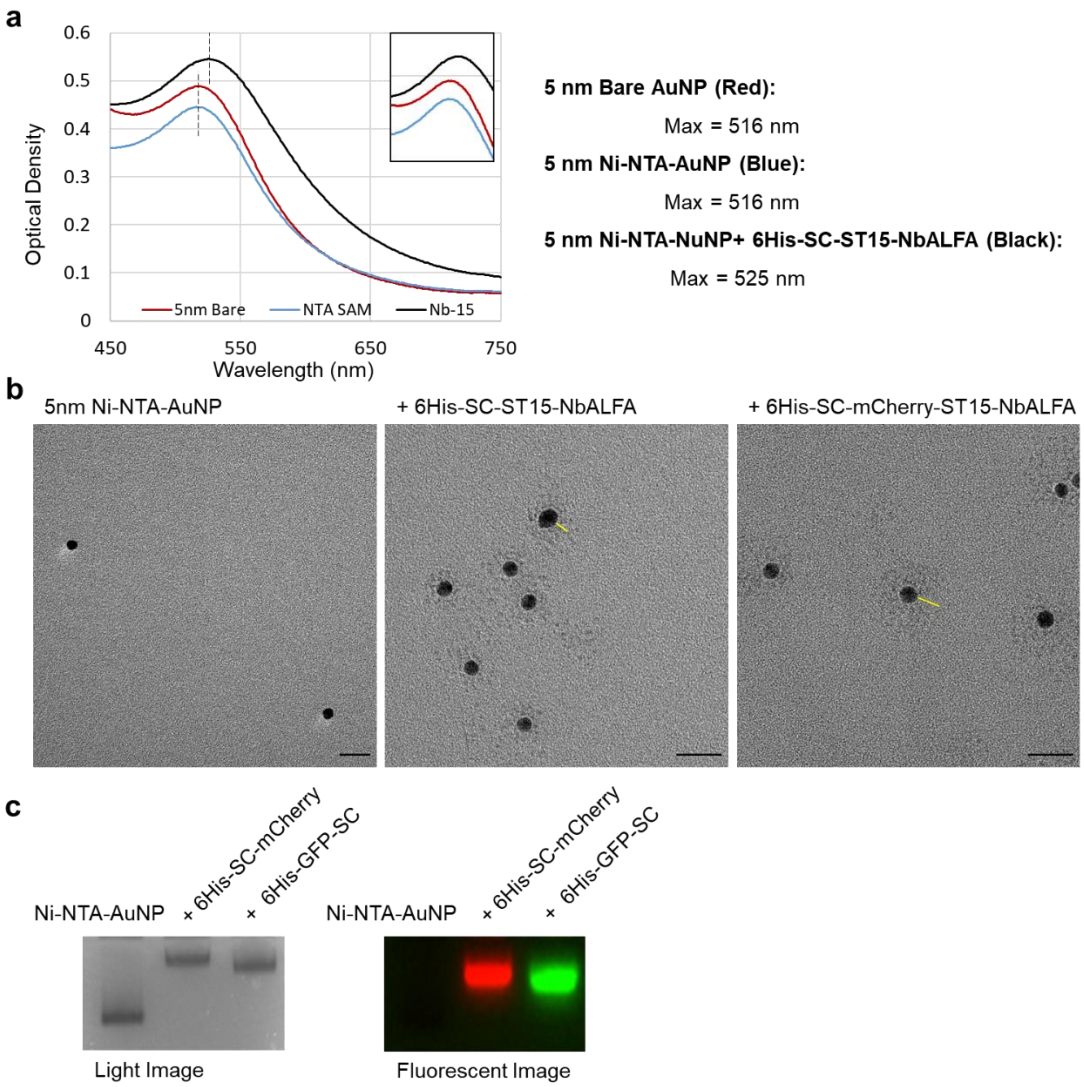

Figure S6. 6His-SC-STn protein chain wrapping on 5 nm Ni-NTA-AuNPs. (a) Surface plasmon resonance spectra of 5 nm AuNPs with different surface conjugation coatings. Maximum absorbance wavelengths are indicated. (b) TEM images of AuNPs with different surface conjugation coatings: 5 nm Ni-NTA-AuNP (left), 5 nm Ni-NTA-AuNP + 6His-SC-ST15-NbALFA (middle) and 5 nm Ni-NTA-AuNP + 6His-SC-mCherry-ST15-NbALFA (right). Yellow lines denote protein layers around AuNPs. Scale bars = 20 nm. (c) Agarose gel light (left) and fluorescent (right) images of Ni-NTA-AuNPs binding to protein chains with 6His-SC-mCherry and 6His-GFP-SC repeating units.

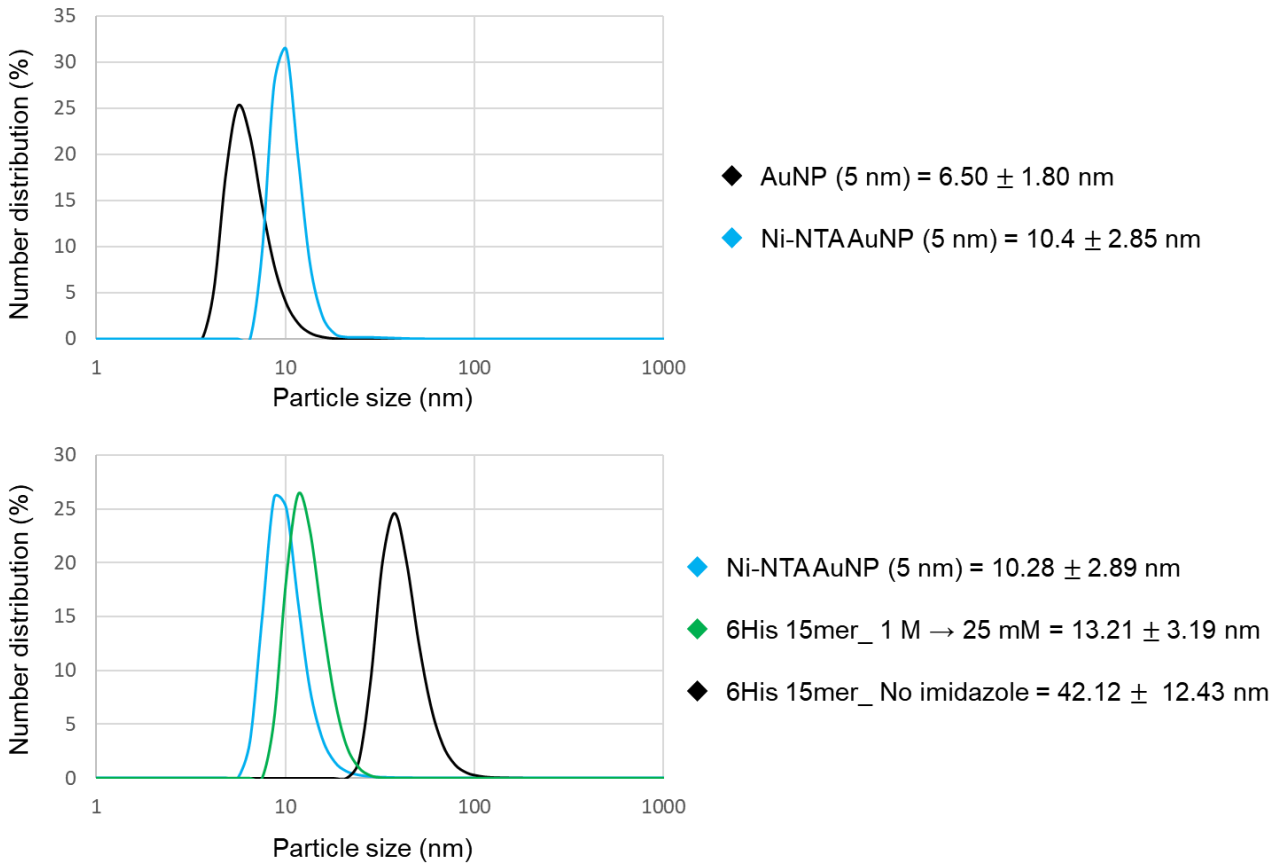

Figure S7. DLS analysis of protein chain wrapping on 5 nm Ni-NTA-AuNPs. (a) DLS size profiles of bare 5 nm AuNP (black) and Ni-NTA covered AuNP (blue). (b) DLS size profiles of Ni-NTA-AuNP (blue) and 6His 15mer protein chain conjugated Ni-NTA-AuNPs with imidazole dialysis (1 M to 25 mM) (green) or without imidazole (black).

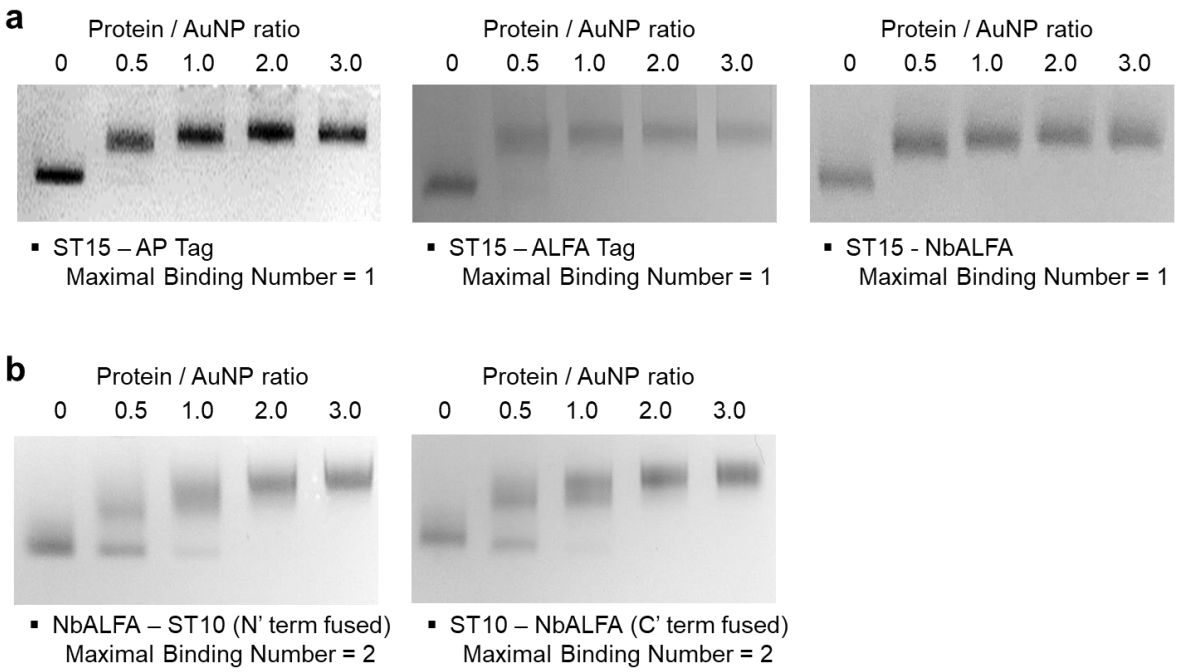

Figure S8. Agarose gel shift analysis of 5 nm Ni-NTA-AuNP binding to 6His-SC-STn proteins with different lengths and fused functional proteins at varying protein:particle ratios.. (a) 5 nm Ni-NTA-AuNP bound with 6His-SC-ST15 scaffold proteins with different functional proteins. Left: SUMO-AP Tag, middle: ALFA Tag, right: NbALFA. (b) 5 nm Ni-NTA-AuNP bound with 6His-SC-ST10 scaffold proteins with an NbALFA moiety on either N-(left) or C-(right) terminus.

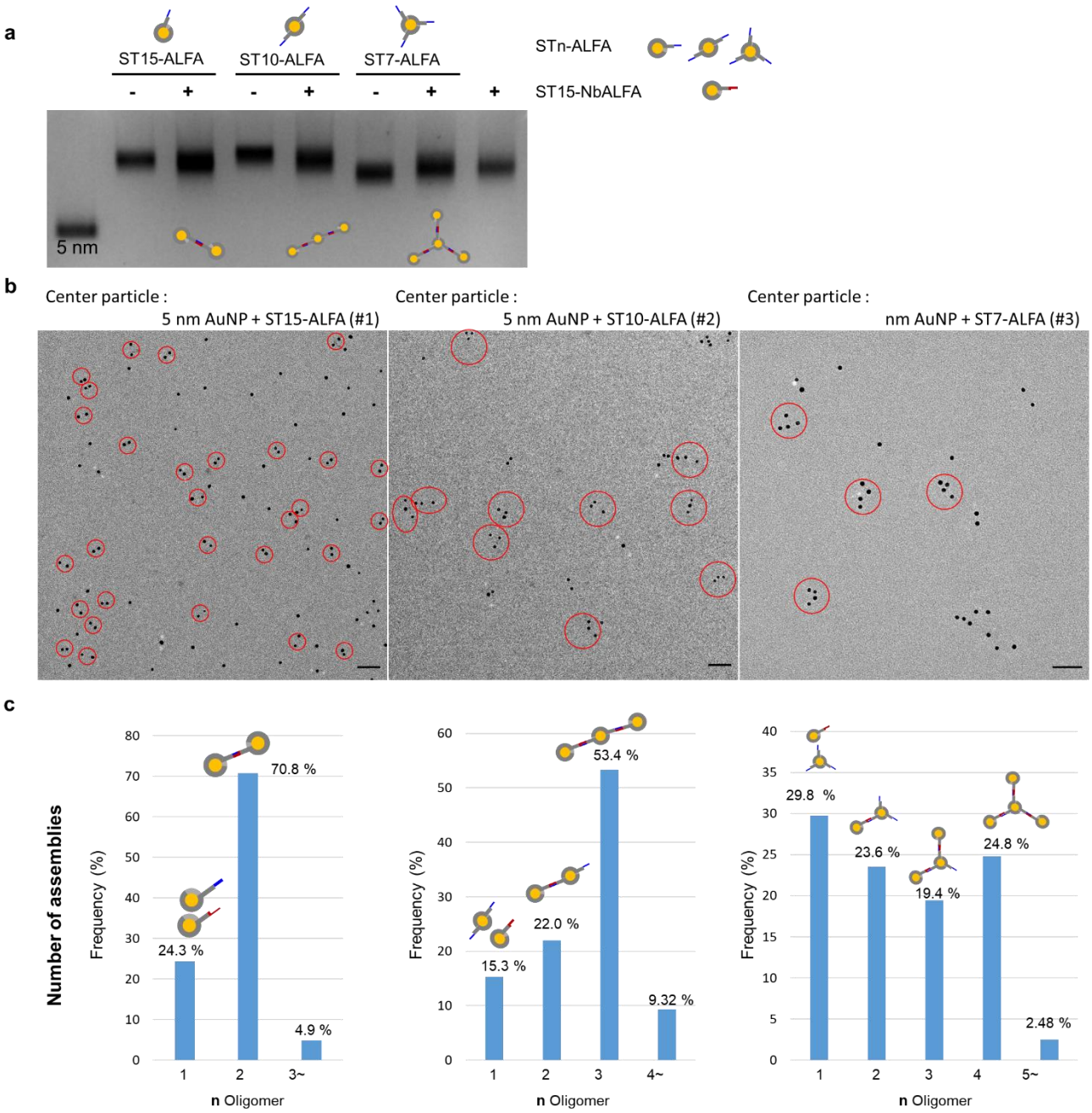

Figure S9. Validation of protein chain valences on AuNPs through particle-particle assemblies: (mono-, di-, tri-valent) 5 nm ALFA-AuNP + monovalent 5 nm NbALFA-AuNP. (a) An agarose gel image of monovalent 5 nm NbALFA-AuNP binding to (mono-, di-, tri-valent) 5 nm ALFA-AuNPs (binding for 1 hr before analysis). (b) Wide field TEM images of particle-particle assemblies. Center particles were monovalent 5 nm ALFA-AuNP (left), divalent 5 nm ALFA-AuNP (middle), and trivalent 5 nm ALFA-AuNP (right). Fully assembled particles are indicated with red circles. Scale bars = 50 nm. (c) Population graphs of particle assemblies (n oligomer). Relative frequencies are obtained based on numbers of particle assemblies (not individual particles). Over 100 particles in TEM images were examined, and particles that are separated by less than 20 nm were considered as assembled.

Supplementary Note I: The 20 nm limit is determined based on the estimated maximal distance between assembled particles: two NTA layers, an NbALFA-ALFA Tag complex, and two $EAAAK_4$ linkers (linker sequences at the end of Supplementary Information). The NbALFA-ALFA Tag complex size is estimated from PDB (6I2G; NbALFA: Green color protein, ALFA Tag: orange color peptide). The pair-distribution of dimers (monovalent NbALFA-AuNP + monovalent ALFA-AuNP) in the inter-particle distance is shown in the below graph, where the average distance is 8.14 nm.

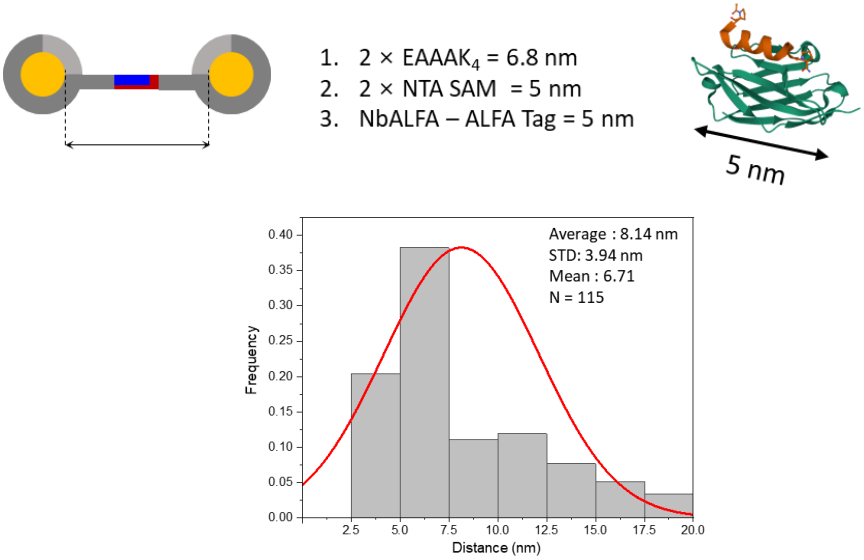

Supplementary Note II: Relative frequencies in Figure S9c are calculated based on numbers of particle assemblies not individual particles. In this case, we can assess relative assembly numbers on center (mono-, di-, and tri-valent) ALFA-AuNPs. One problem is that free monomeric particle papulations are exaggerated by counting both free center ALFA-AuNPs and NbALFA-AuNPs. Therefore, actual assembly efficiency between monovalent ALFA-AuNPs and monovalent NbALFA-AuNPs (Figure S9c right) is higher than 70.8%. Below graphs show relative populations by counting individual particle numbers instead of counting particle assembly numbers.

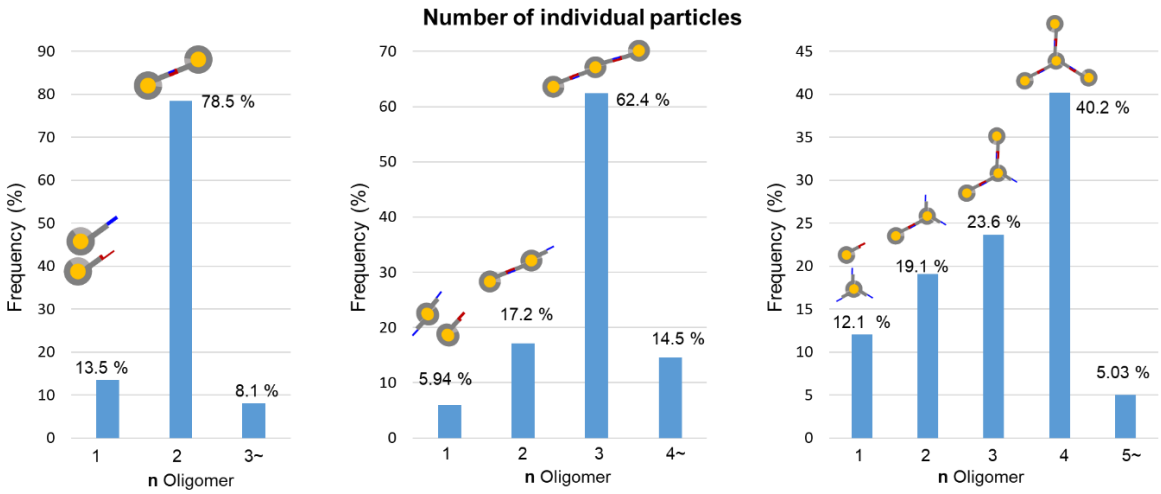

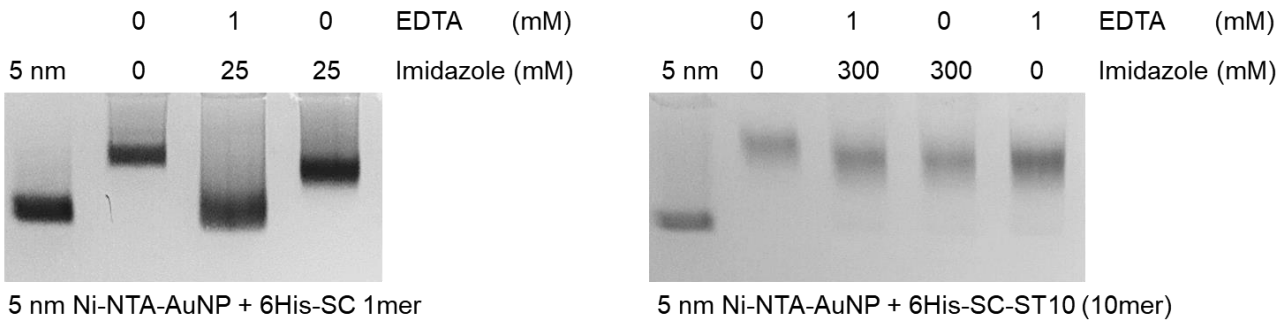

Figure S10. Stability of protein chain wrapping on 5 nm Ni-NTA-AuNP. 5 nm Ni-NTA-AuNP was covered by 6His-SC monomer (left) or by 6His-SC-ST10 (10 mer) (right) and treated with indicated concentrations of imidazole or EDTA before agarose gel analysis.

Supplementary Note: EDTA higher than 1 mM destabilized AuNPs, leading to particle aggregation likely due to deformation of the Ni-NTA layer on AuNP.

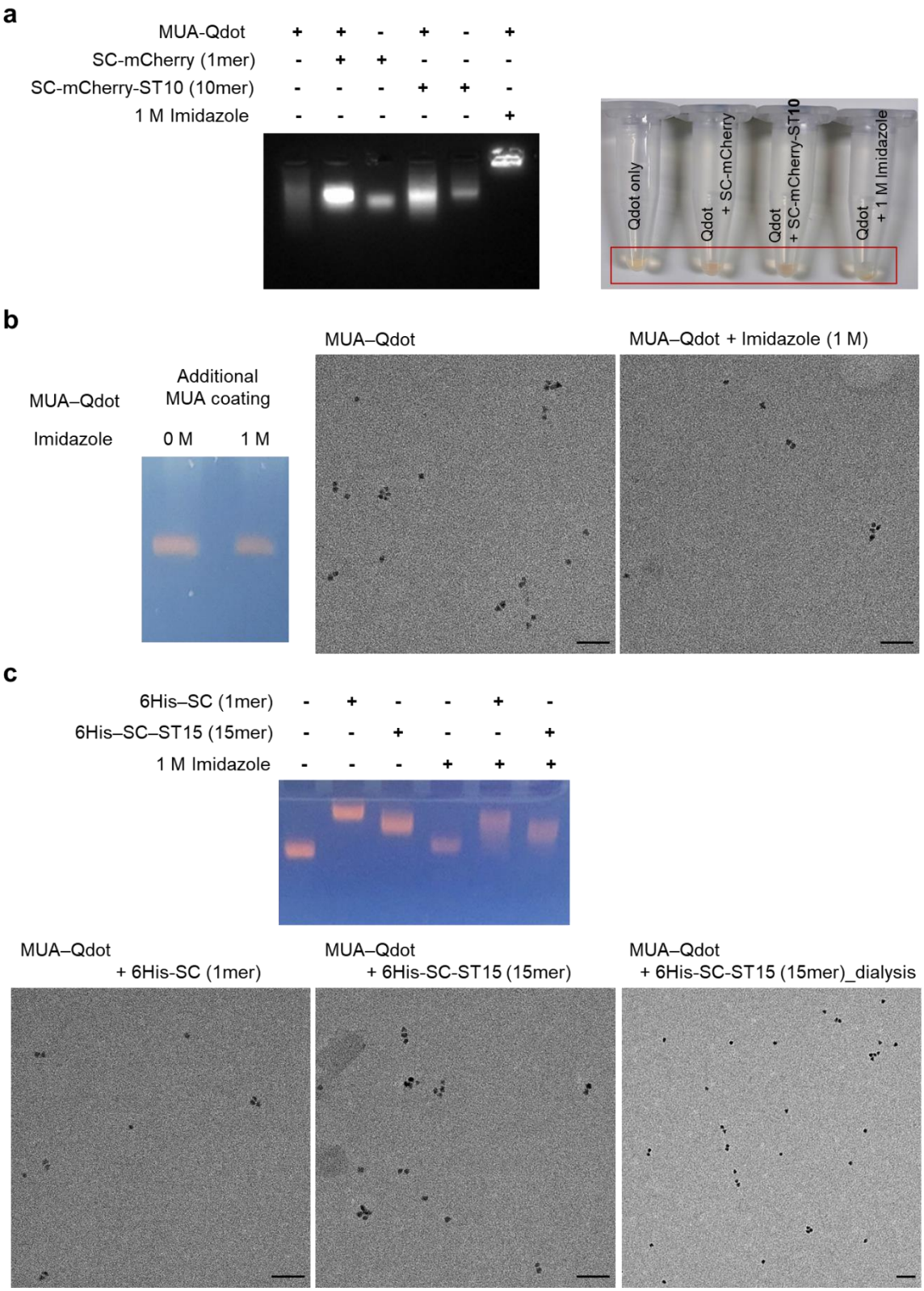

Figure S11. Protein chain wrapping on ~5 nm MUA-Qdot. (a) Agarose gel image and picture of purchased MUA-Qdots treated with 6His-SC-mCherry, SC-mCherry-ST10 (6His 10mer), or 1 M imidazole. The agarose gel was imaged with mCherry and Qdot signals. (b) Agarose gel and TEM images of additionally MUA-covered Qdots with or without 1 M imidazole. (c) Agarose gel and TEM

images of additionally MUA-covered Qdots conjugated with 6His-SC (1mer) or 6His-SC-ST15 (15mer) with or without slow imidazole decrease by dialysis. All scale bars 50 nm.

Supplementary Note: Purchased Qdots were aggregated with 1 M imidazole, staying on a well during electrophoresis (Fig. S11a). Iron oxide nanoparticles were similarly aggregated by 1 M imidazole (data not shown). After additional MUA covering on purchased Qdots, gel and TEM images of the resulting Qdots were not altered by 1 M imidazole (Fig. S11b). Gel and TEM images of MUA-Qdots were not altered by protein or protein chain conjugation (Fig. S11c).

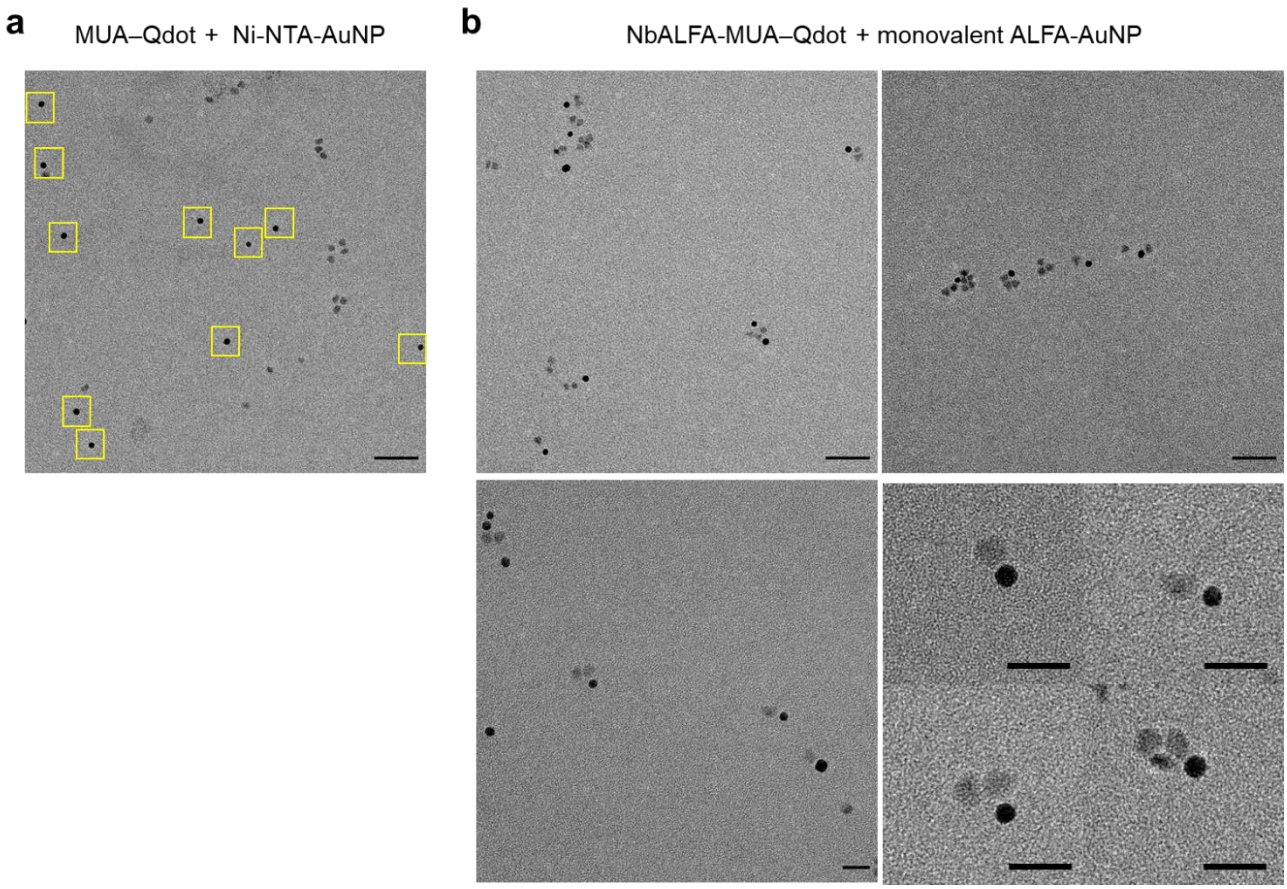

Figure S12. Assembly of protein chain covered MUA-Qdot with monovalent 5 nm AuNP. (a) TEM image of a mixture of MUA-Qdot and 5 nm Ni-NTA-AuNP. Darker and more spherical AuNPs are indicated with yellow boxes. Scale bar 50 nm. (b) TEM images of a mixture of NbALFA-Qdots and monovalent 5 nm ALFA-tag-AuNPs. MUA-Qdots were conjugated to NbALFA-fused 6His 15mer. Enlarged TEM images of Qdot-AuNP assemblies are shown (bottom right). Scale bars 50 nm (top), 20 nm (bottom).

Supplementary Note: MUA-Qdots and 5 nm Ni-NTA-AuNPs are individually dispersed (Fig. S12a). Monovalent 5 nm ALFA-tag-AuNPs monovalently bind to NbALFA-Qdots (Fig. S12b).

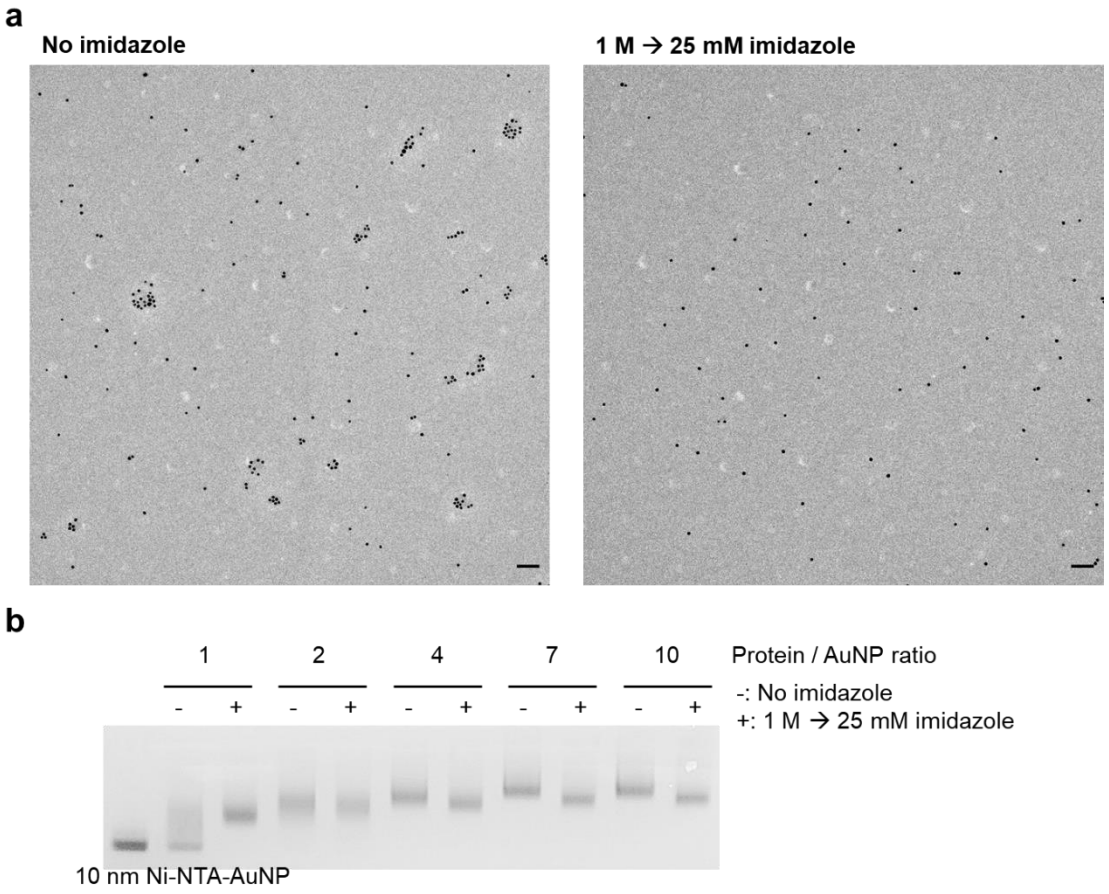

Figure S13. Protein chain wrapping conditions on 10 nm Ni-NTA-AuNP. (a) Wide field TEM images of 10 nm Ni-NTA-AuNP binding to 6His 15mer without imidazole (left) or with slowly decreasing imidazole concentration (from 1 M to 25 mM) at protein:particle ratio 1:1. Scale bars = 50 nm. (b) Agarose gel analysis of 10 nm Ni-NTA-AuNP binding to 6His 15mer without imidazole or with slowly decreasing imidazole concentration (from 1 M to 25 mM) at varying protein:particle ratios.

Supplementary Note: Protein-particle bands for 'No imidazole' are generally higher than those for '1M → 25 mM imidazole', which could indicate a higher number of protein chain binding to particles as well as particle clustering without imidazole during conjugation.

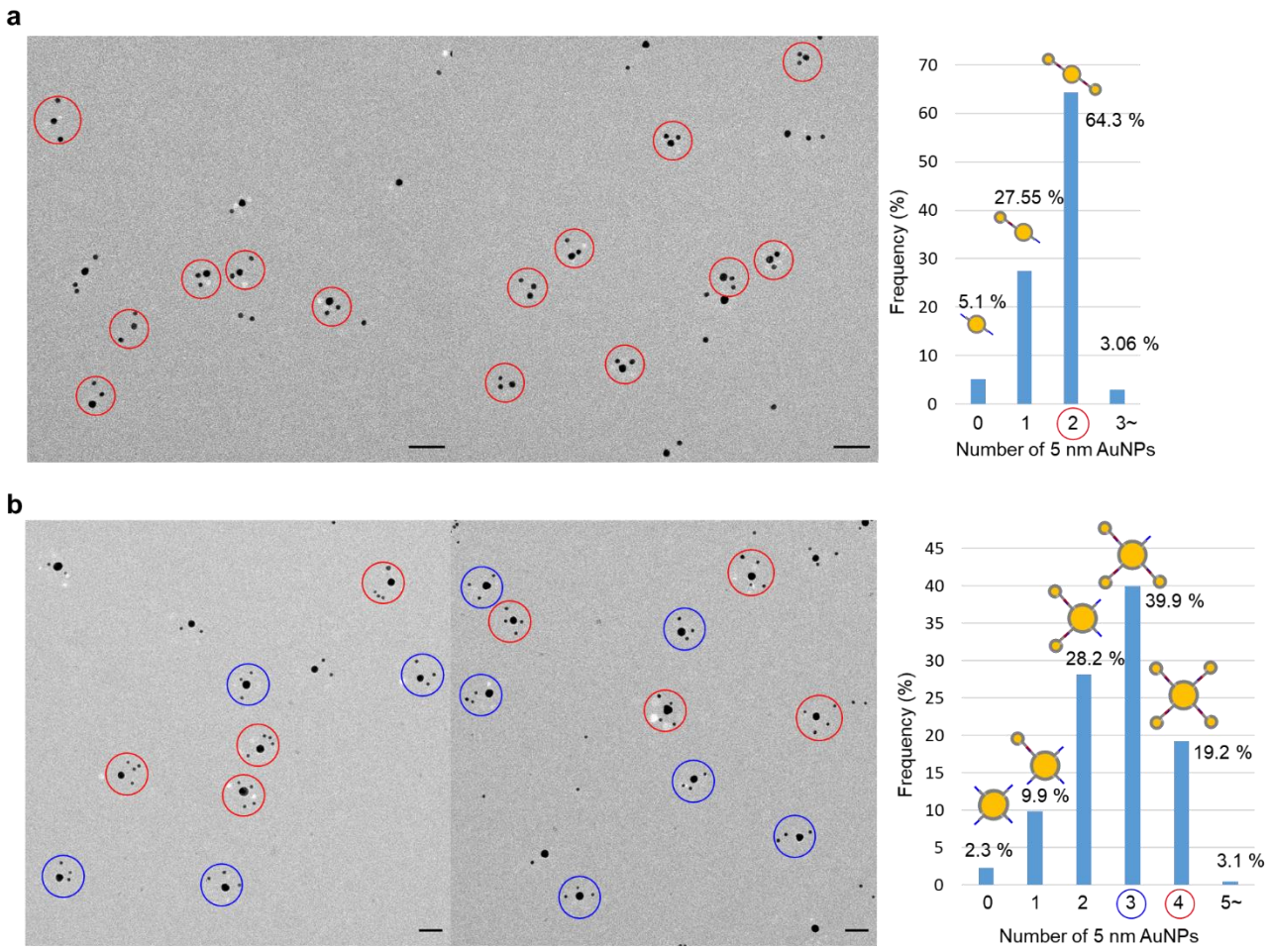

Figure S14. Valance-controlled protein chain conjugation to particles with different sizes: (a) divalent 10 nm ALFA-AuNP or (b) tetravalent 15 nm ALFA-AuNP + monovalent 5 nm NbALFA-AuNP. Wide field TEM images of AuNP assemblies are shown. The graph (right) indicates the relative frequency of 10 nm or 15 nm AuNPs with indicated numbers of bound 5 nm AuNPs around larger center particles. Over 100 particles in TEM images were examined, and particles that are separated by less than 20 nm were considered as assembled. Particle assemblies with indicated numbers of 5 nm AuNPs were indicated with red and blue circles. Scale bars = 50 nm.

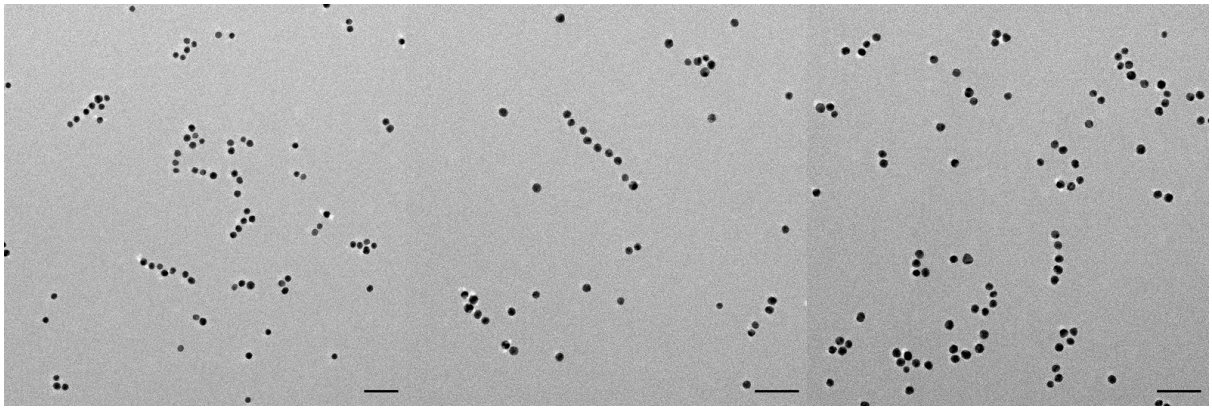

Figure S15. Linear particle-particle assembly: divalent 10 nm ALFA-AuNP + divalent 5 nm NbALFA-AuNP. Wide field TEM images of assemblies between divalent 10 nm NbALFA-AuNP and divalent 10 nm ALFA-AuNP are shown. Scale bars = 50 nm.

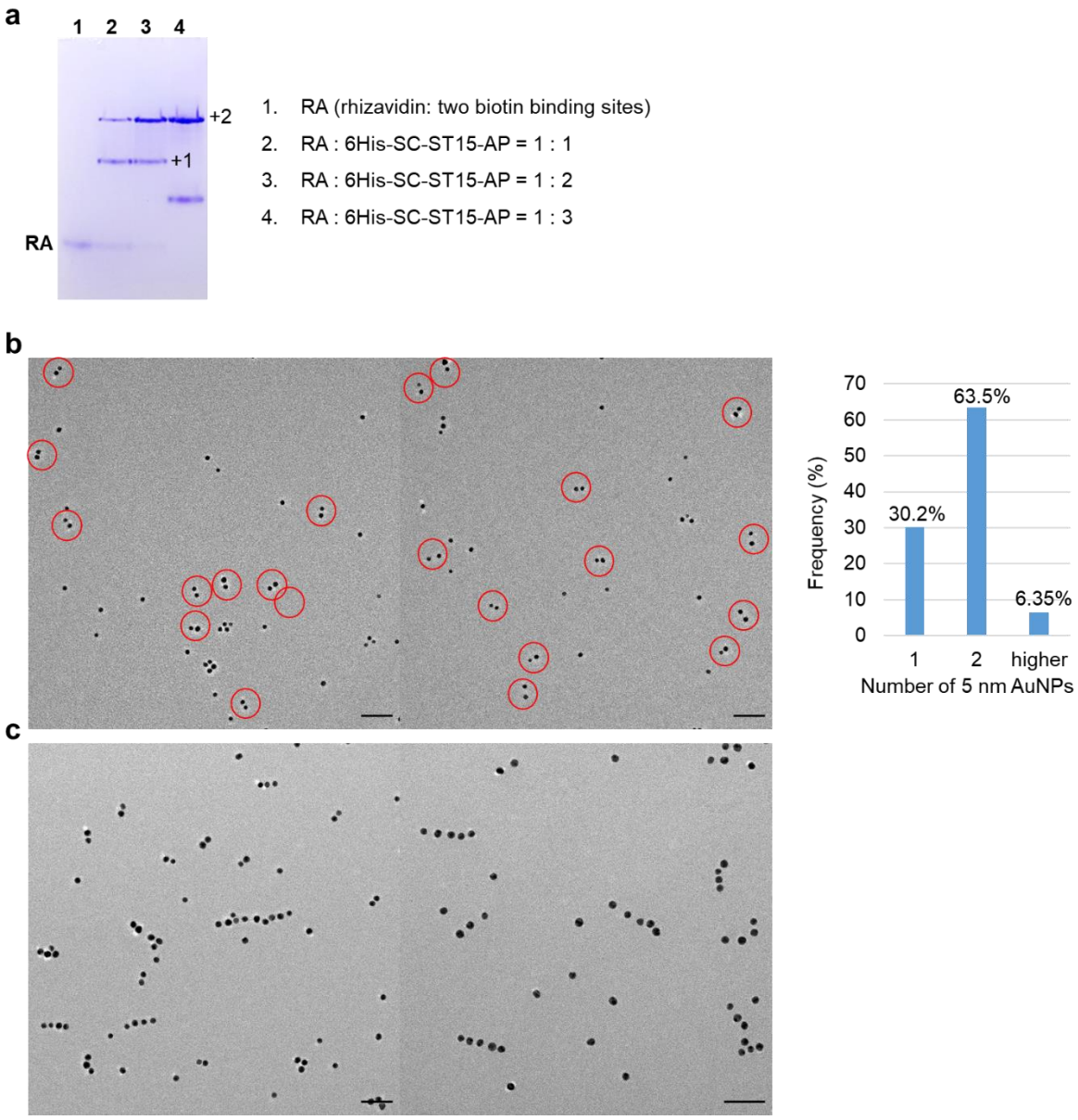

Figure S16. Particle-protein assembly: Rhizavidin (RA) + biotinylated AuNP. (a) Native gel analysis of Rhizavidin (RA) binding to biotinylated protein chain 6His-SC-ST15-AP. Numbers of bound protein chains onto RA gel bands are indicated. (b) Wide field TEM images of monovalent 5 nm biotin-AuNP binding to RA under a 1:2 ratio of particle:RA. Dimeric particle assemblies on RA were indicated with red circles. The graph (right) indicates the relative frequency of 5 nm biotin-AuNP assemblies. Scale bars = 50 nm. (c) Wide field TEM images of divalent 10 nm biotin-AuNP binding to RA. Scale bars = 50 nm.

Supplementary Note: At the 1:2 RA:6His-SC-ST15-AP ratio, RA is not fully bound with two protein chains as shown in Figure S16a, possibly due to steric hindrance of protein chains around relatively small RA, which might also limit dimeric biotin-AuNP assembly on RA.

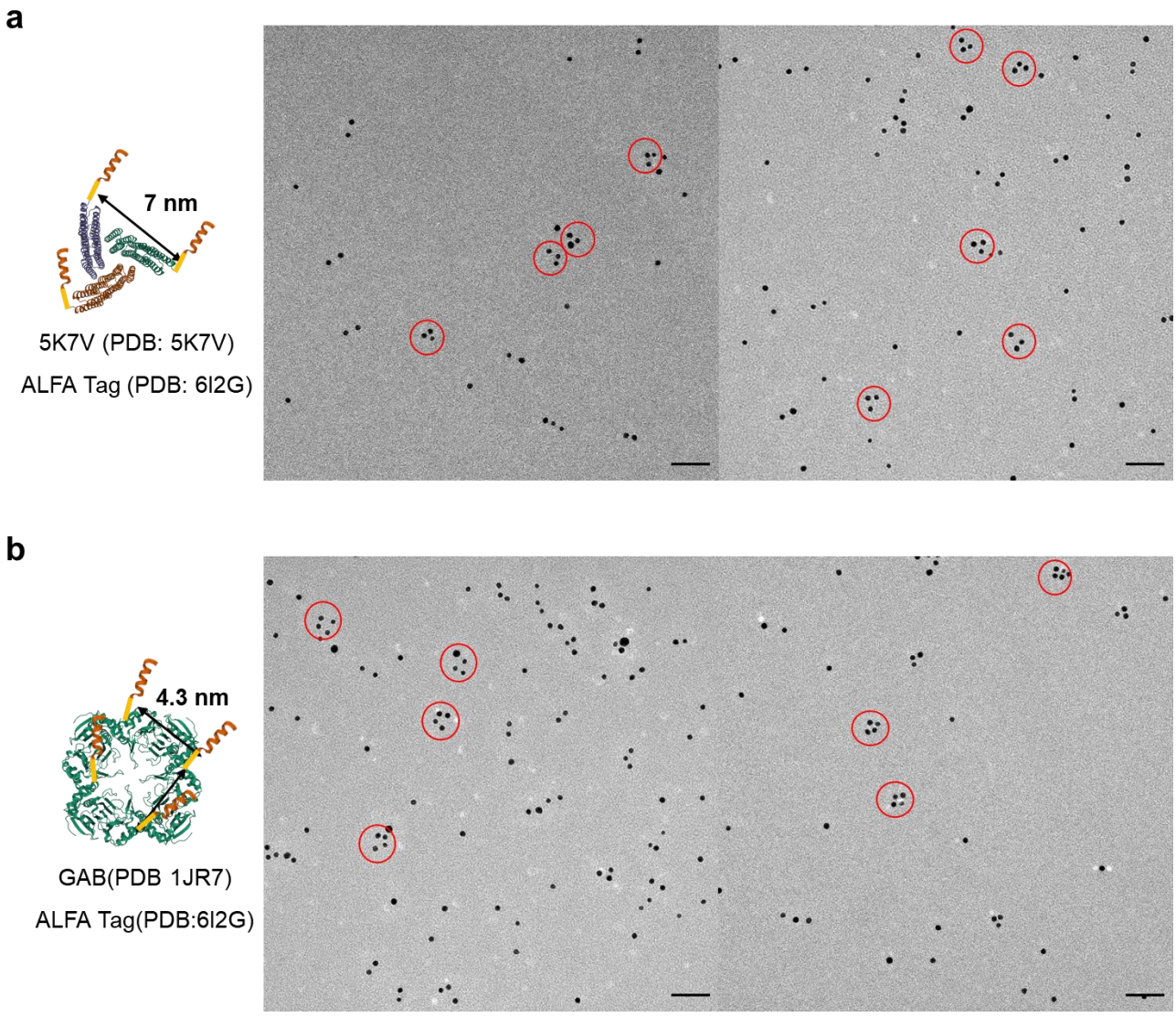

Figure S17. Particle assembly on multimeric proteins: ALFA Tag-multimer + monovalent 5 nm NbALFA-AuNP. (a) The schematic structure of the ALFA tag-fused trimeric (5K7V) protein multimer (left) and wide field TEM images (right) of monovalent 5 nm NbALFA-AuNP binding to ALFA tag fused 5K7V. (b) The schematic structure of the ALFA tag-fused tetrameric (GAB) protein (left) and wide field TEM images (right) of monovalent 5 nm NbALFA-AuNP binding to ALFA tag fused GAB. Distances between ALFA tags on protein multimers are indicated based on PDB structures. Fully assembled triangular or rectangular AuNP clusters are indicated with red circles. Scale bars = 50 nm.

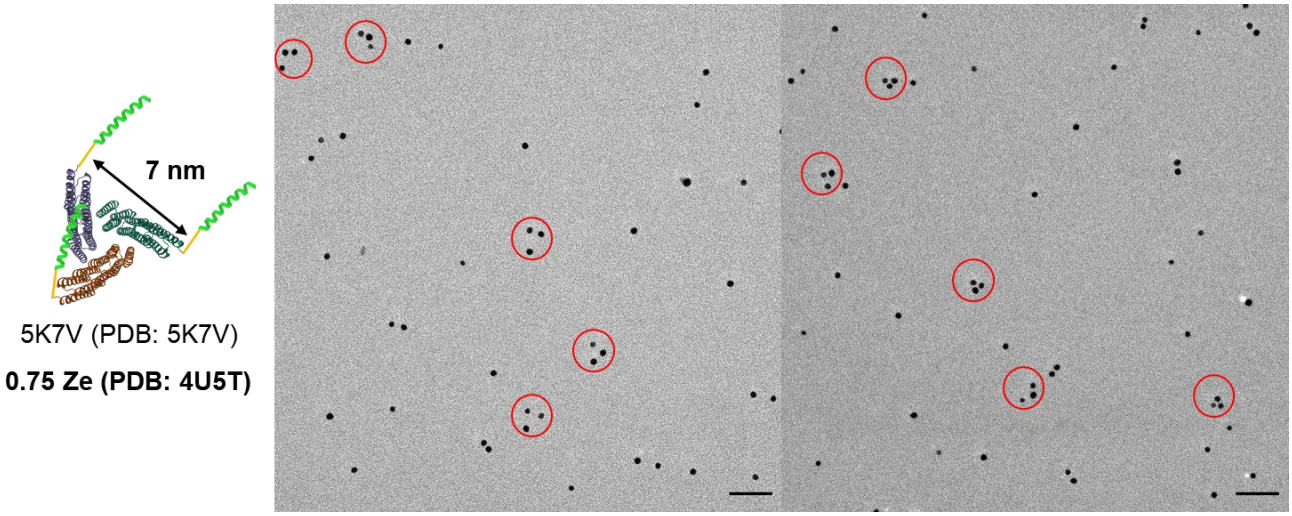

Figure S18. Particle assembly on multimeric proteins: Z_E-trimer (5K7V) + monovalent 5 nm Z_R-AuNP. The schematic structure of the (leucine zipper) Z_E tag-fused trimeric (5K7V) protein (left) and wide field TEM images (right) of monovalent 5 nm Z_R-AuNP binding to Z_E tag-fused 5K7V. The distance between Z_E tags on trimeric 5K7V is indicated based on PDB structures. Fully assembled triangular AuNP clusters are indicated with red circles. Scale bars = 50 nm.

Experimental Methods

Materials. Bare gold nanoparticles (AuNPs, 5 nm, 10 nm, 15 nm) were purchased from BBI Solutions (Cardiff, UK). HS-$(CH_2)_{11}$-EG_3-OCH_2-COOH and HS-$(CH_2)_{11}$-EG_3-NTA was purchased from Prochimia (Sopot, Poland). Iron oxide nanoparticle was purchased from Sigma-Aldrich (#7255331) and mercaptoundecanoic acid (MUA) stabilized CdSe/ZnS quantum dot was purchased from CD Bioparticles (DNQ-M012). Carbon-coated copper grids were purchased from Ted Pella. Agarose was purchased from Duchefa.

Preparation of NTA covered gold nanoparticles. The purchased AuNPs (5 nm, 10 nm, 15 nm, 20 nm) were centrifuged to remove the existing buffer and resuspended in pure tertiary distilled water. Transferred AuNPs were concentrated by centrifugation (40 μL), and HS-$(CH_2)_{11}$-EG_3-NTA (Prochimia) was added to a final 2 mM concentration. Gold nanoparticles were then incubated for more than 16 hr under room temperature for stable SAM formation. The AuNPs were stored at this stage until the next step (particle-protein association) proceeds.

Plasmid construction. The SpyTag tandem repeat genes (STn) with functional binding proteins (NbALFA, ALFA Tag, Z_E, Z_R) were cloned into either pET-28a or pETK-21a (Novagen) expression vector. SpyCatcher proteins were cloned in pET-28a. To construct the site-specifically biotinylated ST tandem repeat sequence, the biotinylation peptide sequence (GLNDIFEAQKIEWHE, AP tag) was added to the N-terminus of the ST tandem repeat sequence. The SUMO protein sequence was inserted between the AP tag and the ST repeat sequence to improve expression and to provide space between biotin and a repeat protein chain. The gene for this proteins was cloned into the pProExHTa (Invitrogen) expression vector.

Protein preparation. All ST tandem repeat scaffold proteins (STn), scaffold proteins (5K7V, GAB) and SC fused proteins were expressed in *E. coli* BL21 (DE3) cells. The transformed cells were grown at 37 °C until OD_{600} = 0.6, and proteins were induced by 1 mM isoprophyl- β -D-thiogalactopyranoside (IPTG), followed by additional incubation (STn scaffolds, Z_E, Z_R and SC: 37 °C, 5 hr; 5K7V: 17 °C, overnight; GAB: 30 °C, 5 hr; NbALFA and ALFA: 23°C, overnight). Induced cells were collected by centrifugation and lysed by sonication in the His binding buffer (500 mM Nacl, 50 mM Tris pH 8.0). After sonication-based breakage of induced cells, clarified cell lysates were applied for purification by 6His-binding (Ni-IDA) columns.

Biotin-SUMO-ST repeat proteins were was expressed in AVB101 (Avidity), an *E.coli* B strain (hsdR, lon11, SulA1) containing a pACYC184 plasmid, which produces biotin ligase BirA upon IPTG induction. Transformed AVB101 cells were grown in the presence of 50 μM biotin, and protein

expression was induced by adding IPTG at the final concentration of 1 mM, followed by additional incubation for 5 hr at 30 °C. After sonication-based breakage of induced cells, clarified cell lysates were purified by the same procedure as described in other non-biotinylated proteins.

Rhizavidin was also expressed in *E. coli* BL21 (DE3) cells. The transformed cells were grown at 37 °C until OD_{600} = 0.9, and proteins were induced by 1 mM IPTG, followed by additional incubation for 4 hr at 37 °C. The induced cells were suspended in PBS containing 1% Triton X-100. After sonication-based breakage, inclusion bodies were isolated from these cell lysates. The inclusion body pellets were dissolved in 6 M guanidinium hydrochloride (GuHCl) pH 1.5. Proteins in GuHCl were refolded by rapid dilution into PBS at 4 °C, and the resulting solutions were stirred overnight. Refolded proteins were again purified by 6His-binding columns.

Construction of tandem repeat protein chains. Over three fold excess 6His-SC protein was reacted with ST tandem repeat scaffold proteins. After 4 hr incubation at room temperature, protein mixtures were dialyzed at a washing solution for a His-binding column (50 mM Tris pH 8.0, 500 mM NaCl, 50 mM imidazole). Multi-his tag protein scaffolds were re-associated with Ni-IDA beads with gentle shaking under room temperature for 10 min. Un-reacted SC was then excluded by harsh washing (180 mM imidazole). Finally, multi 6His protein chains were eluted with an elution buffer (50 mM Tris pH 8.0, 250 mM NaCl, 500 mM imidazole).

Protein chain binding to AuNPs. For Ni charging on AuNPs, 200 μL of a particle buffer (30 mM Tris pH 7.8) was added to NTA-AuNP. Ni^{2+} solution was added to the solution as final 40 mM, then incubated with gentle shaking for 10 min. After shaking, solution was centrifuged (13,000 rpm, 15 min) to precipitate Ni-NTA-AuNPs. Supernatants were removed, and AuNP pellets were resuspended in a buffer containing 30 mM Tris pH 7.8, Glycine 19.2 mM. For protein chain binding to AuNPs, protein chains were mixed with Ni-NTA-AuNPs with desired ratios under 1 M imidazole. Protein-particle mixtures were then dialyzed into a buffer containing 30 mM Tris pH 7.8 and 25 mM imidazole. Unbound proteins were eliminated by centrifuge.

Gel analysis of protein bound particles. 1.5 ~ 2 % agarose gels were used for gel electrophoresis. Gold nanoparticle solutions containing 5% sucrose were introduced to gels, and the gels were run at full voltage for at least 15 min. The Takara's Mupid-2Plus was used. The running buffer was 0.5x TA buffer. The images of gels were recorded using either digital camera or Chemi-Doc (Biorad).

TEM Image. A 10 μL sample solution with 0.5% sucrose was deposited on a copper grid for a minute, after which excess solution was wicked away with a filter paper. After deposition, the grid was washed with 10 μL 30 mM Tris (pH 7.8) twice. To confirm the configuration of a specific band, a band on

agarose gel was cut, and a TEM grid was located at the cut aperture. Gold nanoparticles were then adsorbed to the grid through 60 sec of additional gel electrophoresis. Electron micrographs were acquired using Tecnai G2 F30 S-Twin microscope at 300 kV. Most of TEM images were acquired without negative staining. For the detection of protein layers, particle-protein conjugates were stained for 60 sec with 2% uranyl acetate.

DLS Measurements. DLS analysis of all AuNP suspensions were performed using a Zetasizer Nano ZS DLS system (Malvern Instruments Ltd., England). For particle size determination, 1 mL aliquots of solution were placed in disposable polystyrene covets and analyzed at 25 ºC. DLS measurements were performed using Non-invasive Back Scatter (NIBS) with a scattering angle of 173° in air and 10 scans of 10 s per sample taken.

Protein Sequences

Spycatcher003

MGSSHHHHHHSSGLVPRGSHMGAMVTTLSGLSGEQGPSGDMTTEEDSATHIKFSKRDEDGR
ELAGATMELRDSSGKTISTWISDGHVKDFYLYPGKYTFVETAAPDGYEVATPIEFTVNEDGQ
VTVDGEATEGDAHT

Spycatcher-mCherry

HMGAMVDTLSGLSSEQGQSGDMTIEEDSATHIKFSKRDEDGKELAGATMELRDSSGKTIST
WISDGQVKDFYLYPGKYTFVETAAPDGYEVATAITFTVNEQGQVTVNGKATKGDAHIGSMV
SKGEEDNMAIIKEFMRFKVHMEGSVNGHEFEIEGEGEGRPYEGTQTAKLKVTKGGPLPFAW
DILSPQFMYGSKAYVKHPADIPDYLKLSFPEGFKWERVMNFEDGGVVTVTQDSSLQDGEFIY
KVKLRGTNFPSDGPVMQKKTMGWEASSERMYPEDGALKGEIKQRLKLKDGGHYDAEVKT
TYKAKKPVQLPGAYNVNIKLDITSHNEDYTIVEQYERAEGRHSTGGMDELYK

GFP – Spycatcher

HMKGEELFTGVVPILVELDGDVNGHEFSVRGEGEGDATIGKLTLKFICTTGKLPVPWPTLVTT
LTYGVQCFSRYPDHMKRHDFFKSAMPEGYVQERTISFKDDGKYKTRAVVKFEGDTLVNRIE
LKGTDFKEDGNILGHKLEYNFNSHDVYITADKQENGIKAEFTVRHNVEDGSVQLADHYQQN
TPIGDGPVLLPDNHYLSTQTVLSKDPNEKRDHMVLHEYVNAAGITGSGAMVDTLSGLSSEQ
GQSGDMTIEEDSATHIKFSKRDEDGKELAGATMELRDSSGKTISTWISDGQVKDFYLYPGKY
TFVETAAPDGYEVATAITFTVNEQGQVTVNGKATKGDAHIENLYFQGLEHHHHHH

Rhizavidin (RA)

MFDASNFKDFSSIASASSSWQNQSGSTMIIQVDSFGNVSGQYVNRAQGTGCQNSPYPLTGRV
NGTFIAFSVGWNNSTENCNSATGWTGYAQVNGNNTEIVTSWNLAYEGGSGPAIEQGQDTFQ
YVPTTE

5K7V–ALFA Tag

HMIEEVVAEMIDILAESSKKSIEELARAADNKTTEKAVAEAIEEIARLATAAIQLIEALAKNLAS
EEFMARAISAIAELAKKAIEAIYRLADNHTTDTFMARAIAAIANLAVTAILAIAALASNHTTEE
FMARAISAIAELAKKAIEAIYRLADNHTTDKFMAAAIEAIALLATLAILAIALLASNHTTEEFM

AKAISAIAELAKKAIEAIYRLADNHTSPTYIEKAIEAIEKIARKAIKAIEMLAKNITTEEYKEKA
KSAIDEIREKAKEAIKRLEDNRTGSAEAAAKEAAAKEAAAKEAAAKAGSGGS**PSRLEEELR**
RRLTEP

GAB–ALFA Tag

HMGQDYSGFTLTPSAQSPRLLELTFTEQTTKQFLEQVAEWPVQALEYKSFLRFRVAKILDDLC
ANQLQPLLLKTLLNRAEGALLINAVGVDDVKQADEMVKLATAVAHLIGRSNFDAMSGQYYA
RFVVKNVDNSDSYLRQPHRVMELHNDGTYVEEITDYVLMMKIDEQNMQGGNSLLLHLDD
WEHLDNYFRHPLARRPMRFAAPPSKNVSKDVFHPVFDVDQQGRPVMRYIDQFVQPKDFEE
GVWLSELSDAIETSKGILSVPVPVGKFLLINNLFWLHGRDRFTPHPDLRRELMRQRGYFAYA
SNHYQTHQGGSAEAAAKEAAAKEAAAKEAAAKAGSGGS**PSRLEEELRRRLTEP**

5K7V – 3/4 Z_E

HMIEEVVAEMIDILAESSKKSIEELARAADNKTTEKAVAEAIEEIARLATAAIQLIEALAKNLAS
EEFMARAISAIAELAKKAIEAIYRLADNHTTDTFMARAIAAIANLAVTAILAIAALASNHTTEE
FMARAISAIAELAKKAIEAIYRLADNHTTDKFMAAAIEAIALLATLAILAIALLASNHTTEEFM
AKAISAIAELAKKAIEAIYRLADNHTSPTYIEKAIEAIEKIARKAIKAIEMLAKNITTEEYKEKA
KSAIDEIREKAKEAIKRLEDNRTGSGGGGSGGGGS**ENTALETEVAELEQEVQRLENIVSQY**
RTRYGPL

STn – AP Tag (n = 10, 15)

*** AP – SUMO = Blue (AP Tag = Bold)**

TPSYYHHHHHHDYDIPTTENLYFQGAME**GLNDIFEAQKIEWHE**MSDSEVNQEAKPEVKPE
VKPETHINLKVSDGSSEIFFKIKKTTPLRRLMEAFAKRQGKEMDSLRFLYDGIRIQADQTPED
LDMEDNDIIEAHREQIGGATYGS

[AHIVMVDAYKPDGDGDGDGDGLVPRGS] × n (10, 15)

KPLRGAVFSLQKQHPDYPDIYGAIDQNGTYQNVRTGEDGKLTFKNLSDGKYRLFENSEPAGY
KPVQNKPIVAFQIVNGEVRDVTSIVPQDIPATYEFTNGKHYITNEPIPPKLEHHHHHH

STn – ALFA Tag (n = 7, 10, 15)

HM [AHIVMVDAYKPDGDGDGDGDGLVPRGS] × n (10, 15)

AEAAAKEAAAKEAAAKEAAAKAGSGGS**PSRLEEELRRRLTEP**

NbALFA – STn (n = 10, 15)

EVQLQESGGGLVQPGGSLRLSCTASGVTISALNAMAMGWYRQAPGERRVMVAAVSERGNA
MYRESVQGRFTVTRDFTNKMVSLQMDNLKPEDTAVYYCHVLEDRVDSFHDYWGQGTQVT
VSSGGSGSAEAAAKEAAAKEAAAKEAAAKAGS

[AHIVMVDAYKPDGDGDGDGDGLVPRGS] × n (10, 15)

KPLRGAVFSLQKQHPDYPDIYGAIDQNGTYQNVRTGEDGKLTFKNLSDGKYRLFENSEPAGY
KPVQNKPIVAFQIVNGEVRDVTSIVPQDIPATYEFTNGKHYITNEPIPPKLEHHHHHH

STn – NbALFA (n = 6, 10)

HM [AHIVMVDAYKPDGDGDGDGDGLVPRGS] × n (6, 10)

AEAAAKEAAAKEAAAKEAAAKAGSGGSEVQLQESGGGLVQPGGSLRLSCTASGVTISALNA
MAMGWYRQAPGERRVMVAAVSERGNAMYRESVQGRFTVTRDFTNKMVSLQMDNLKPED
TAVYYCHVLEDRVDSFHDYWGQGTQVTVSS